

PSFC/JA-11-48

**Upgrade of the MIT Linear Electrostatic Ion  
Accelerator (LEIA) for nuclear diagnostics  
development for Omega, Z and the NIF**

N. Sinenian, M. J.-E. Manuel, A.B. Zylstra, M. Rosenberg, C. J.  
Waugh, H. G. Rinderknecht, D. T. Casey, H. Sio, J. K.  
Ruszczynski, L. Zhou, M. Gatu Johnson, J. A. Frenje, F. H. Seguin,  
C. K. Li, R. D. Petrasso, C. L. Ruiz\* and R. J. Leeper.\*

\* Sandia National Laboratories, Albuquerque, NM 87185, USA

April, 2012

**Plasma Science and Fusion Center  
Massachusetts Institute of Technology  
Cambridge MA 02139 USA**

This work was supported in part by Sandia National Laboratory (Agreement No. 611557), National Laser User's Facility (DOE Award No. DE-NA0000877), Fusion Science Center (Rochester Sub Award PO No. 415023-G), US DOE (Grant No. DE-FG52-09NA29553), Laboratory for Laser Energetics (LLE) (No. 414090-G), Lawrence Livermore National Laboratory (No. B580243). Reproduction, translation, publication, use and disposal, in whole or in part, by or for the United States government is permitted.

**Upgrade of the MIT Linear Electrostatic Ion Accelerator (LEIA) for nuclear diagnostics development for Omega, Z and the NIF**

N. Sinenian,<sup>a)</sup> M. J.-E. Manuel, A. B. Zylstra, M. Rosenberg, C. J. Waugh, H. G. Rinderknecht, D. T. Casey, H. Sio, J. K. Ruszczyński, L. Zhou, M. Gatu Johnson, J. A. Frenje, F. H. Séguin, C. K. Li, and R. D. Petrasso

*Plasma Science and Fusion Center, Massachusetts Institute of Technology,  
Cambridge, MA 02139, USA*

C. L. Ruiz and R. J. Leeper

*Sandia National Laboratories, Albuquerque, NM 87185,  
USA*

(Dated: 5 April 2012)

The MIT Linear Electrostatic Ion Accelerator (LEIA) generates DD and D<sup>3</sup>He fusion products for the development of nuclear diagnostics for Omega, Z and the National Ignition Facility (NIF). Significant improvements to the system in recent years are presented. Fusion reaction rates, as high as  $10^7 \text{ s}^{-1}$  and  $10^6 \text{ s}^{-1}$  for DD and D<sup>3</sup>He, respectively are now well regulated with a new ion source and electronic gas control system. Charged fusion products are more accurately characterized, which allows for better calibration of existing nuclear diagnostics. In addition, in-situ measurements of the on-target beam profile, made with a CCD camera, is used to determine the metrology of the fusion-product source for particle-counting applications. Finally, neutron diagnostics development has been facilitated by detailed MCNP modeling of neutrons in the accelerator target chamber, which is used to correct for scattering within the system. These recent improvements have resulted in a versatile platform, which continues to support the existing nuclear diagnostics while simultaneously facilitating the development of new diagnostics in aid of the National Ignition Campaign at the National Ignition Facility.

PACS numbers: 29.20.Ba, 29.27.-a

---

<sup>a)</sup>nareg@psfc.mit.edu

## I. INTRODUCTION

The National Ignition Campaign (NIC) seeks to achieve thermonuclear ignition and energy gain of a laser-compressed DT fuel pellet at the National Ignition Facility (NIF).<sup>1,2</sup> Essential to this effort is the availability of robust nuclear diagnostics for the measurement of key parameters, including the neutron yield ( $Y_n$ ), areal density of the fuel ( $\rho R$ ) and the ion temperature ( $T_{ion}$ ). Such measurements allow fine-tuning of target and laser parameters in addition to assuring the experimental community that positive progress is being made towards ignition.

Nuclear diagnostics development at national laboratories and national user laser facilities such as Omega<sup>3,4</sup> can be costly in terms of the potential time and money spent in debugging and developing an instrument. In this vein, smaller facilities such as the MIT Linear Electrostatic Ion Accelerator (LEIA), shown in Fig. 1, allow tests of new ideas, development of new diagnostics and calibration of existing nuclear diagnostics on a continual basis at a fraction of the cost. Valuable time at laser facilities is thus available for target physics and experiment validation rather than diagnostic development. It is important that small facilities such as LEIA are accurately calibrated with the precision required for inertial confinement fusion (ICF) diagnostics development applications.

In this context, the LEIA<sup>5-7</sup> has been significantly improved through a series of hardware and software upgrades over the last three years. In addition, LEIA has been better characterized through experimental calibrations and simulations, which has provided greater accuracy and precision required for advanced diagnostics development for Omega, Z and the NIF. The implementation of a new ion source and gas control system has allowed for better control of the spatial and temporal characteristics of the fusion-product source, which is essential for the calibration of a number of nuclear diagnostics. In addition, the development of a CCD-camera based target viewing system (TVS), combined with modeling of neutron scattering within the target chamber, has allowed for detailed characterization of the fusion-product source; this has further facilitated the development of neutron yield diagnostics. Finally, a newly-implemented multi-channel analyzer (MCA) with advanced signal-processing algorithms has been used to measure charged-fusion products more accurately and with greater precision; these benefits directly propagate to the energy calibration of charged-particle spectrometers and have opened the door for new physics studies. In addi-

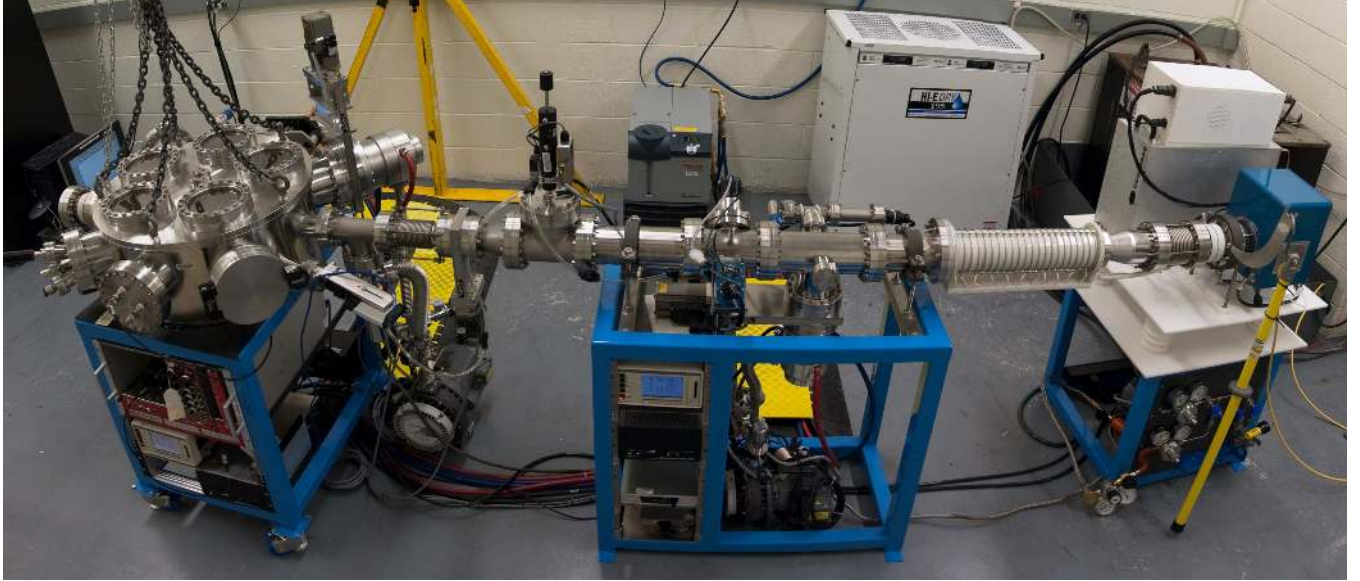


FIG. 1. The MIT Linear Electrostatic Ion Accelerator (LEIA). Shown, from left to right, are the cylindrical target chamber, beam line with in-situ beam diagnostics, including a faraday cup and a beam profiler, and ion source, enclosed in the blue shroud at the right.

tion to the added diagnostic development capabilities, the facility has provided very valuable hands-on training for a number of graduate and undergraduate students; these students are the main contributors to this work.

This paper is organized as follows: Section II gives the reader an overview of the various hardware components of the accelerator, along with a discussion of recent improvements; section III discusses the software development undertaken for both data acquisition, control and simulation capability; section IV discusses some recent development work on diagnostics currently in use at Omega and the NIF; section V describes the future direction of LEIA.

## II. LEIA OVERVIEW AND HARDWARE DEVELOPMENT

A complete schematic of the upgraded LEIA is shown in Fig. 2. The upgrades include a new radio-frequency (RF) driven positive ion source, an open-air high voltage deck, reconfigured beamline, and target chamber. The newly implemented ion source, manufactured by National Electrostatics Corp.(NEC),<sup>8</sup> is capable of producing  $200 \mu\text{A}$  deuteron beams and  $170 \mu\text{A}$   $^3\text{He}$  ion beams. A terminal voltage of 150 kV, generated using a Cockroft-Walton Multiplier (not shown in the schematic), accelerates these ions onto a target downstream.

The target, composed of a copper substrate with a thin film of  $\text{ErD}_2$ , is loaded with either D or  $^3\text{He}$  to allow production of either DD or  $\text{D}^3\text{He}$  fusion products.

### A. Implementation of a New Ion Source

A new ion source, schematically shown in Fig. 2, was acquired and implemented to enhance beam control and stability. The  $\text{D}_2$  (or  $^3\text{He}$ ) plasma discharge is generated within the source using a capacitively-coupled 300 watt RF oscillator operating at 100 MHz. The source also includes permanent magnets and an Einzel lens assembly. The plasma is first compressed by magnetic fields at the entrance to an aluminum canal (1 or 2 mm diameter) where it is electro-statically extracted and focused to a downstream target. The source may be biased using up to three power supplies for operation, excluding the RF oscillator power supply: one each for the focus, the extractor and the probe electrodes; these supplies are referenced to the terminal voltage (deck bias). Note the probe and extractor electrodes, shown in Fig. 3, located upstream and downstream of the plasma bottle, respectively. In these types of sources, the purpose of the probe power supply is to drive ions out of the source by maintaining a potential difference between the extractor and the probe electrodes; for this reason it is typically referenced to the extractor bias using an isolation transformer. This approach was not taken as it does not allow a single digital electronic controller to readily control and monitor the supplies because they have large (several kV) DC offsets between them. The approach taken here was to reference all three supplies to the terminal voltage and to compensate for this by adding an offset voltage to the probe output equal to the instantaneous extractor bias. This output tracking between supplies was achieved in software. Nevertheless, any reference to the probe bias in this work refers to a potential difference between the extractor and probe electrodes. Three supplies were obtained from Glassman HV Inc.<sup>9</sup> for this application: two MK-series supplies, with 15 kV and 20 kV outputs for the focus and probe, respectively, and an MJ-series power supply with an output of 5 kV for the extractor. These supplies are housed in the source supply box shown in Fig. 2. That box also incorporates an Acromag ES2152<sup>10</sup> fiber-optic-coupled controller, which drives and monitors the analog interfaces of the supplies while providing a single digital, fiber-isolated interface to the control computer. The bias conditions depend strongly on the electrostatic optics of the entire system. For this system, an extractor bias of 0-5 kV,

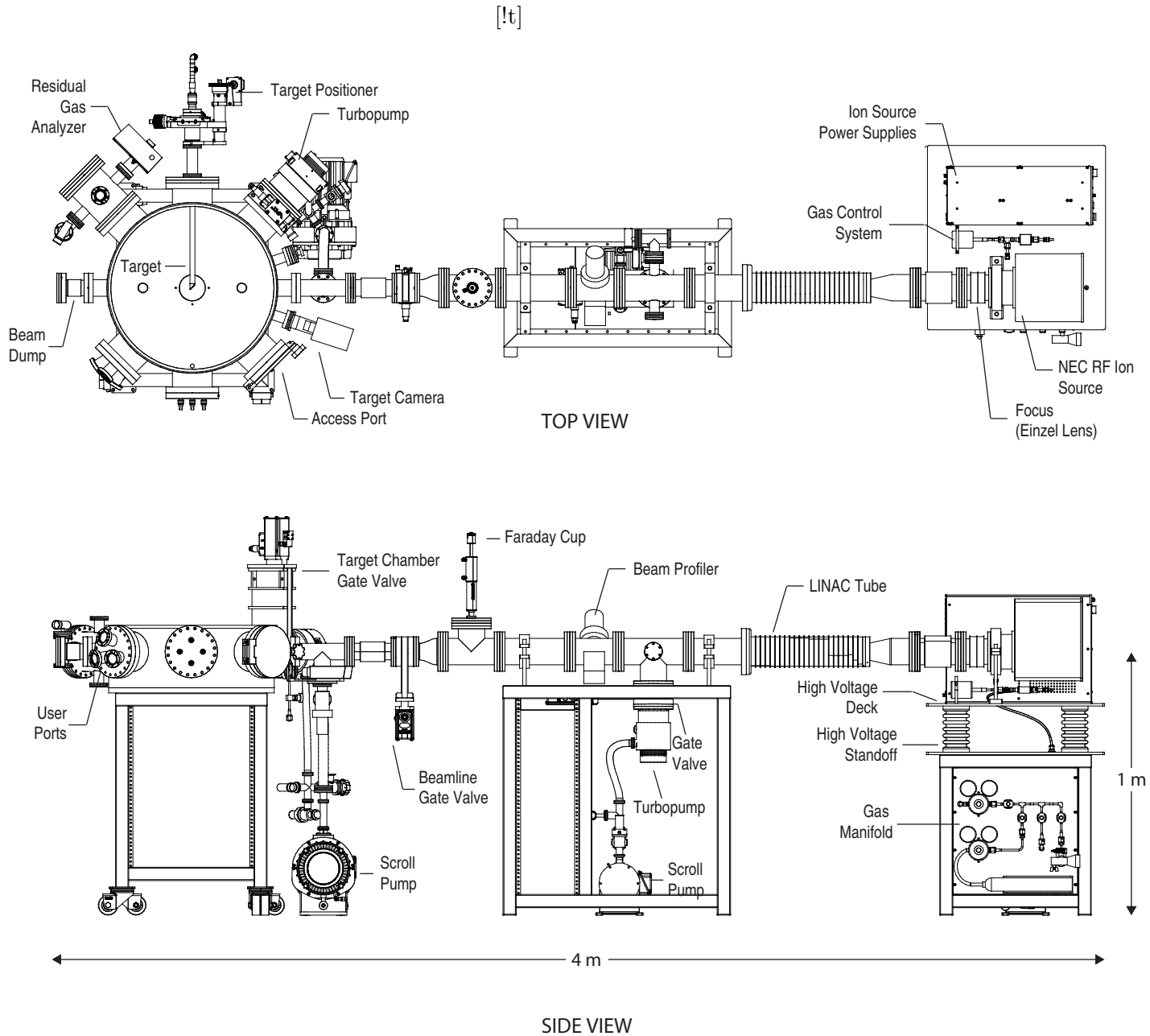


FIG. 2. Top and side view of LEIA. Shown are the target chamber, beamline and ion source along with supporting components. Electrostatic components include a focusing lens and a linear accelerating tube. Beam diagnostics include a faraday cup, beam profiler and a residual gas analyzer. The vacuum system is comprised of two turbopumps and three dry vacuum (scroll) pumps.

a focus of  $\sim 3\text{-}10$  kV and a probe of  $\sim 3\text{-}10$  kV proved to be sufficient for extracting and focusing a beam of ions down to a diameter of 3 mm approximately 2.5 m downstream of the ion source. It was found that the optimal probe and focus values depend on the extractor bias. The extractor, despite its name, does not actually drive ions out of the source. It biases the entire source relative to the terminal voltage, and thus provides an extra potential drop for ions after they exit the source. The terminal voltage drops across a linear accelerating (LINAC) tube, composed of a series of polished metallic rings insulated by ceramic (the LINAC is shown in Fig. 2). It is an adiabatic focusing lens since the large voltage gradient ( $3\text{ kV}\cdot\text{cm}^{-1}$ ) is opposite the direction of beam propagation. In order to focus a beam farther downstream, it is necessary to introduce some de-focusing in the optics, upstream of the accelerating tube; this leads to the requirement of a several kV potential increase from the extractor to the focus electrodes. The defocusing occurs within the Einzel lens, which has an effective bias equal to the difference between the focus and extractor. Consequently, as the extractor is varied, this difference must be maintained for a given focal point. Since the LINAC tube is located just downstream of the ion source ( $\sim 20$  cm), it was found that a grounded extractor (hence the probe bias alone) was sufficient to drive ions out of the source and into the LINAC tube. For a grounded extractor, probe and focus voltages of  $\sim 4$  kV and  $\sim 3$  kV were required for proper focusing.

The stability of the fusion reaction rate depends strongly on the stability of the ion beam current; the latter is a function of the ion source bottle pressure. The nominal flow rate of gas into the source is approximately  $0.02$  sccm/s with a nominal fill pressure in the range of  $10 - 30$  mTorr.<sup>8</sup> It was found that momentary fill pressures greater than 50 mTorr were often required for proper startup of the plasma and that the optimal fill pressure during operation range extended out to approximately  $40 - 60$  mTorr. These required flow rates of D are quite low for modern thermal mass-flow controllers. Thus, ion sources of this type often utilize manual or motor-driven variable-leak valves<sup>8</sup> for gas pressure control, whereby the valve orifice is manually set to a fixed position (and adjusted manually as required). Since some diagnostic applications require reliable and steady beam currents over extended periods of time (as discussed in Sec. IV), a fast-response feedback-controlled gas-control system was designed and implemented.

The gas control system consists of a Horiba STEC piezo-electric flow control valve<sup>11</sup> and an MKS 626-series Baratron Capacitance Manometer<sup>12</sup> for direct measurement of the ion

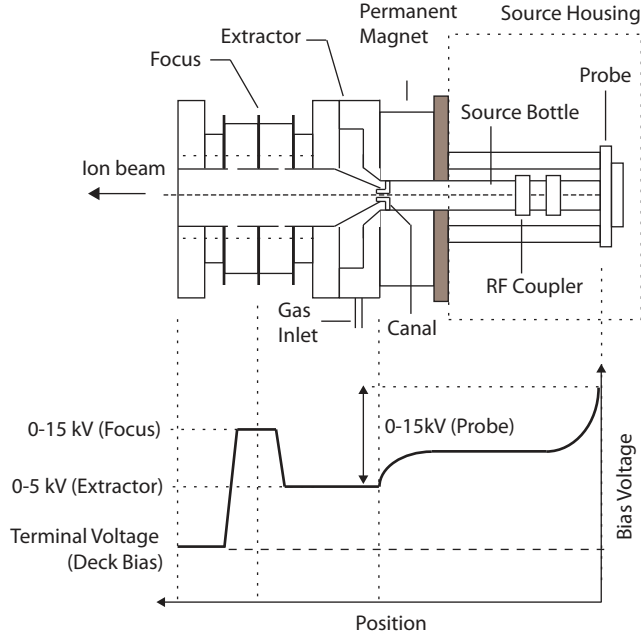


FIG. 3. Schematic of the NEC RF Positive Ion Source, including the probe, extractor and focusing lens assembly. Shown below the source is a sample bias profile. The allowable range of values for each of the bias supplies are indicated and may be adjusted independently.

source fill pressure. The same fiber-optic-coupled controller was used to readout the fill pressure and drive the piezo-electric valve based on commands it received from a software implemented proportional-integral-differential (PID) control loop. The loop allows control of the pressure to within 0.5 mTorr. With proper tuning of the loop, the step response time of the system is  $< 2$  seconds. Since the maximum piezo-valve orifice leads to over-pressurization of the source, the software package implements a valve calibration feature to prevent the valve from being opened too far. This feature is essential since over-pressurization of the source slows down the response time of the gas control system.

The new gas control system has helped to stabilize the beam current and hence the fusion reaction rate. The fusion reaction rate, as inferred by a fixed detector with a finite solid angle, is a function of beam current, beam energy, on-target beam position and the extent to which the target is loaded. We observe, as shown in Fig. 4, small variations in the DD fusion reaction rate over fine timescales. These variations are within the statistical uncertainty of the count-rate measurement ( $\sigma = \pm 2\%$ ). More importantly, no significant long-term (of order 10 - 20 minute) trends are seen in the data when feedback control of the gas pressure is utilized. Various parts of the system, including the ion source canal and



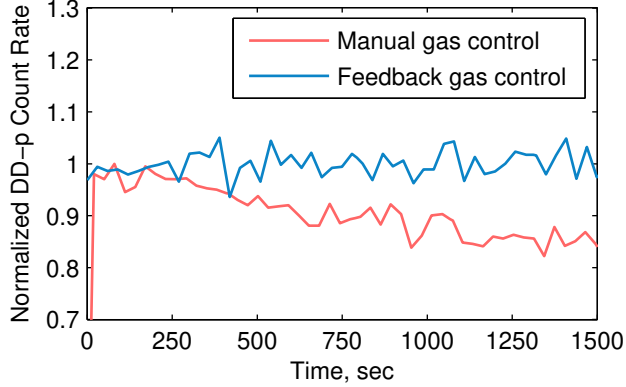


FIG. 4. Stability of the DD-p count rate (normalized to the average count rate for manual control and the max. count rate for feedback control) as a function of time. Variations in the count rate over fine timescales ( $\sim 60$  s) are within the statistical uncertainty of the measurement ( $\sigma = \pm 0.02$ ). Long-time-scale ( $\sim 20$  min) drifts of the count rate are observed when the gas control valve orifice is manually fixed. These drifts were stabilized with the use of feedback gas pressure control.

target, undergo thermal expansion as the source and beam are operated for long duration; any long-term changes in the count-rate associated with system components reaching steady-state operating parameters are mitigated with the use of feedback. For these data, the ion source was allowed to warm-up for several hours per NEC's standard operating procedure; a residual gas analyzer (RGA) was used to verify that the beam predominantly consisted of deuterium. Characterization and control of the fusion reaction rate for long time scales is particularly important for development of neutron yield diagnostics based on activation of materials, as discussed in Sec. IV.

## B. Targets and Target Viewing System

The targets used for LEIA were manufactured by Sandia National Laboratories.<sup>13</sup> The active layer of the targets consists of Erbium-Deuteride ( $\text{ErD}_2$ ) with a diameter of 1 cm and a nominal thickness of  $5 \mu\text{m}$ , corresponding to the range of a  $150 \text{ keV } ^2\text{H}^+$  ion. Although the thickness is sufficient for stopping 150 keV deuterons, it was found that these thin targets deteriorate after approximately 20 hours of beam-on-target time for ion beam powers in the range of 15-20 Watts. The thin layer of  $\text{ErD}_2$  is ablated off, exposing the copper substrate. Future targets will incorporate thicker active layers for increased lifetime and durability.

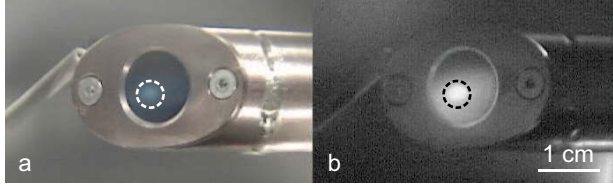


FIG. 5. Images of a 140 keV deuteron beam incident on an  $\text{ErD}_2$  target (a) with ambient lighting and (b) without ambient lighting. Shown in these images are the water-cooled target holder (constructed of copper) and the circular target itself (approx. diameter of 1.1 cm). The ion source was biased with a probe voltage of 8.7 kV, extractor of 5 kV and focus of 9 kV to achieve a focal spot size of approximately 3 mm (dashed circle) on a target 2.5 meters downstream of the ion source.

Other target materials have also been tested, such as titanium and it was found that these targets produced DD fusion rates significantly lower than  $\text{ErD}_2$ .

A new target viewing system (TVS) diagnostic was implemented for in-situ measurements of the on-target beam profile. The target camera, shown in Fig. 2, is a CCD-based network camera (Axis Communications Model 221<sup>14</sup>), which provides a more accurate measurement of the fusion product source size relative to that of the beam profiler. The beam profiler samples the beam cross-section and position well upstream of the target (see Fig. 2) where it is typically broader as it is converging onto the target. The visible light self-emission of energetic deuterons exciting the target medium is sufficient to generate an image without the need for background lighting. The camera utilizes a CCD with a sensitivity of 0.65 lux, which provides sufficient sensitivity for this low-light application. Images of a 140 keV deuteron beam incident on target were taken with the TVS, with and without ambient lighting as shown in Figs. 5a-b. These images were taken during a single run where the beam was focused to a diameter of 3 mm; the source was operated at a fill pressure of 40 mTorr and biased with an extractor of 5 kV, focus of 9 kV and probe of 8.7 kV. Such in-situ measurements of the beam profile allow the operator to point and focus the beam for each run with greater accuracy than one might achieve with a beam profiler alone. Precise knowledge of the fusion source size and position with respect to target chamber center (TCC) is also essential for the calibration of several diagnostics, as discussed in Sec. IV.

### III. SOFTWARE AND SIMULATION DEVELOPMENT

#### A. Control, Monitoring and Logging

The upgrades and modifications to accelerator hardware require a software-based control solution, which is scalable and modular, allowing components of the control software to be re-used, modified or removed entirely in response to hardware changes. To this end, a novel modular and extensible toolkit was developed for control of the various accelerator subsystems. This Modular Control Toolkit (MCT)<sup>15</sup> was written in C++ and uses open-source libraries<sup>16</sup> for its graphical user interface; it currently supports both 32-bit and 64-bit UNIX-like systems. The toolkit itself consists of a central console, a module manager, an interlock engine and a shared library with templates for building modules. The shared library implements the base code which is common to all modules and is hence shared between all running modules. Using the toolkit, one only needs to write a module with the minimal code required to communicate with hardware specific to a given experiment.

Several new modules were written to control the accelerator, including the ion source controller, the vacuum valve controller, the turbopumps, ion gauge controller and other system-level components. Full electronic control, monitoring and logging of the system parameters (e.g. voltages, currents, pressures and temperatures) is now possible.

Improvements were also made to the way system and run parameters are logged. An SQL-based<sup>17</sup> database was implemented to hold run data along with useful information about charged-particle detectors, targets and other system-wide parameters. The terminal voltage, source bias, fusion count rates, fill pressures and charged-particle data are stored for each shot and may be queried over a web interface using any number of fields. This new capability is extremely useful for quickly retrieving run data. The database also serves as an essential aid when debugging the system or resolving anomalies in data, as one has a reference of pertinent system parameters for each experimental run.

#### B. Charged-Particle Diagnostics Suite

The primary data-acquisition system consists of a newly implemented NIM-based setup with four signal chains for the measurement of charged-particle spectra. Surface barrier detectors (SBDs) are routinely used for direct measurements of the energy spectra of charged

fusion products. This data acquisition system consists of a model N1728B multichannel-analyzer, obtained from C.A.E.N.,<sup>18</sup> a four-channel pre-amplifier, and custom software developed in-house, hereon referred to as the C.A.E.N. MCA Application (CMA). The open hardware specifications and implementation details provided by C.A.E.N. have enabled us to acquire charged-particle spectra with greater accuracy and better precision. All aspects of the signal processing chain, from initial analog-to-digital conversion to post-processing and deconvolution of the pre-amplifier impulse response function (IRF) are controlled using custom software written in Java. Deconvolution of the pre-amplifier response is done in real-time in hardware (as originally implemented by C.A.E.N.) using a well-known algorithm.<sup>19</sup> The MIT-developed software package allows the user to specify parameters for the algorithm, trigger and acquisition; simultaneous acquisition of energy spectra and oscillograms of single-particle events are also possible. Furthermore, one may use the CMA to record count rates over time (i.e. software scaler mode), to perform in-situ analysis, including data fitting, and to calibrate and store channel-to-energy mapping data; the stock open-source Java-based software furnished by C.A.E.N. does not implement these latter features, though it was helpful in developing this software suite.

Of particular importance in the new system is the deconvolution of the preamplifier IRF. Ideally, the SBD-preamplifier combination will have a fast-rising “impulse” with an amplitude that is linearly proportional to the energy of the incident particle; the SBD depletion depth ( $\sim 2000\mu\text{m}$ ) is sufficient to stop the charged-particle. In practice, the SBD takes a finite amount of time to sweep out the charge (the electron-hole pairs) generated by the incident particle. The charge sweep-out time increases with incident particle energy, leading to an impulse amplitude that is systematically lower for higher energy particles. Thus, the incident particle energy is underestimated for more energetic particles. This is problematic for 14.7 MeV  $\text{D}^3\text{He}$  protons in the laboratory since calibration of the SBD itself is typically accomplished using low-energy  $\alpha$ -particles from the decay of heavy isotopes, such as  $^{226}\text{Ra}$ .

The energy calibration of the MCA is defined by a linear mapping between channel and incident particle energy. Four  $\alpha$ -particles from a  $^{226}\text{Ra}$  source, with energies in the range of 4 - 8 MeV<sup>20</sup>, are measured using the MCA. The energies of these particles as a function of measured channel, as shown in Fig. 6, are then fit to the form

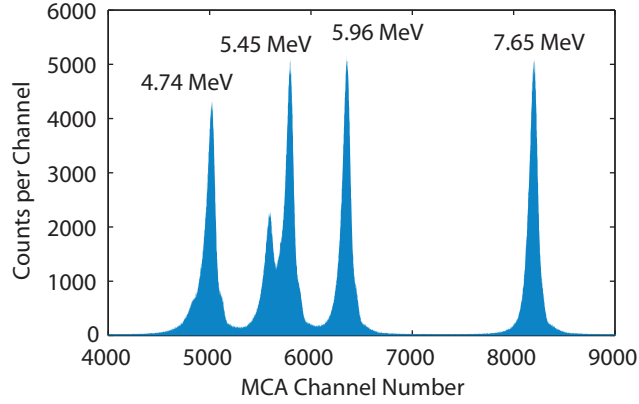


FIG. 6. Spectrum of  $\alpha$ -particles from a  $^{226}\text{Ra}$  source acquired using the charged-particle diagnostics suite. The SBD is exposed to the source under high vacuum without a filter between the source and the SBD. This data is used to define a mapping between incident particle energy and MCA channel.

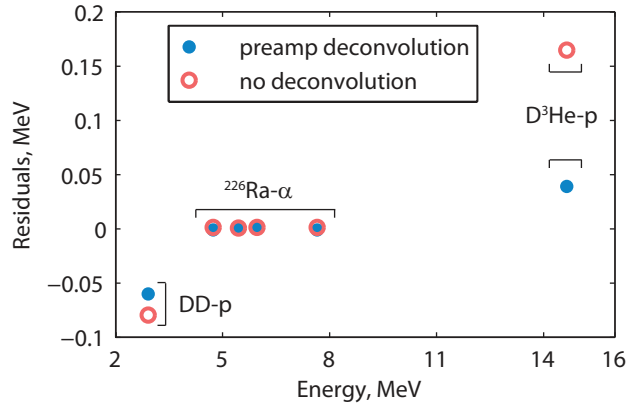


FIG. 7. Comparison of the new and old MCA systems, with and without deconvolution of the preamplifier IRF, respectively. Shown are the residuals of the calibration fit as a function of incident particle energy. The MCA is calibrated to the  $^{226}\text{Ra}$ - $\alpha$ 's (4-8 MeV) and this calibration is then extrapolated to both lower and higher energies. The residuals of the calibration for 3 MeV and 14.7 MeV fusion-protons are significantly lower when the preamplifier IRF is deconvolved in the measurement.

$$E_M = a_1 + a_2 \times N_C \quad (1)$$

where  $N_C$  is the MCA channel,  $E_M$  is the energy of a particle as measured by the MCA, and

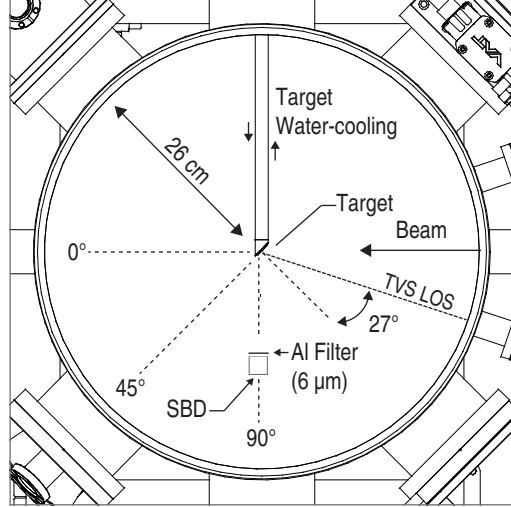


FIG. 8. Schematic of the target chamber, showing the SBD (at  $90^\circ$  with respect to the beam), water-cooled target holder and target (angled at  $45^\circ$ ). The SBD is filtered with a thin layer of light-tight Al (typ.  $6\mu m$ ) to protect the SBD from the large flux of scattered beam ions. Also shown is the line-of-sight (LOS) of the Target Viewing System (TVS), which forms a  $27^\circ$  angle with respect to the normal of the target surface.

$a_1$  and  $a_2$  are the fit coefficients. This calibration fit is extrapolated to both lower energies (e.g. 3 MeV DD-p) and higher energies (e.g. 14 MeV D<sup>3</sup>He-p). The linearity of the MCA is quantified by computing the residual of the fit, defined as

$$R \equiv E_I - E_M \quad (2)$$

where  $E_I$  is the known energy of the  $\alpha$ -particle and  $E_M$  is the energy of the particle as measured by the calibrated MCA. The residual is thus a measure of how much a measured particle energy deviates from the expected particle energy.

These residuals, along with residuals of the 14 MeV and 3 MeV fusion products, are shown in Fig. 7 for two cases: (a) the old MCA system, which does not deconvolve the preamplifier IRF, and (b) the new MCA, which performs hardware deconvolution in real-time. The deconvolution algorithm essentially linearizes the impulse height output of the SBD with respect to incident particle energy, resulting in more accurate measurements (lower residuals). The residuals of the fusion products at 3 MeV and 14.7 MeV are computed using the difference between simulated and measured values of the proton energies at  $90^\circ$  with respect to the ion beam, as shown in Fig. 8. For such charged-particle measurements, a thin aluminum filter

(6  $\mu\text{m}$ ) is used to block SBD from the large flux of low-energy ( $< 140$  keV) scattered beam ions to prevent the SBD from damage. The measured energy spectra are corrected for the charged-particle ranging through this filter. One significant component of the residuals at 3 MeV, and to a lesser extent, at 14.7 MeV, are the uncertainties of the expected energy of fusion products incident on the SBD (at  $90^\circ$ ). These energies are computed by adjusting the birth energies of the fusion products for beam kinematics (discussed in the next section) and ranging down the particle from its birth energy through several microns of the target material,  $\text{ErD}_2$ . The latter correction is complicated by the fact that one must know where reactions occur within the target. This depth is computed in a simulation in which particles are ranged through the appropriate amount of  $\text{ErD}_2$  as they leave the target at a given angle. The energies are simulated to within an accuracy of 10-20 keV. These simulations are discussed in the following section. Another component that adds to the residuals of the fusion products is the precision of the energy measurement, which depends on experimental factors (e.g. how well the SBD position is known); these factors lead to a measurement precision of 20 keV. The major component of the residuals of the 3 MeV and 14.7 MeV fusion products are attributed to these two components, and the total systematic uncertainty of charged-particle energy measurements with this system is  $\pm 50$  keV.

### C. Beam-Target Physics Simulation

Predictive capability of the energy and fluence of fusion products is important for verifying the calibration of the charged-particle diagnostics suite and the associated-particle technique,<sup>21</sup> where one relies on in-situ measurements of the fluence of 3 MeV protons to determine the fluence of the associated 2.45 MeV neutrons from the DD fusion reaction. To this end, a code was developed to simulate beam-target physics, including the slowing down of charged-particle reactants and products, relativistic reaction kinematics, and the differential angular cross-section for the fusion reactions of interest. The simulation takes beam energy, current, species and cross-sectional area as inputs. The beam cross-sectional area may be approximated using either the beam profiler or more accurate CCD data (from the TVS) of beam area on target for a given run. The beam current and area are used to determine fusion reaction rates; the former may be measured using the faraday cup. Note that in lieu of a beam velocity selector, a residual gas analyzer is used to verify that the

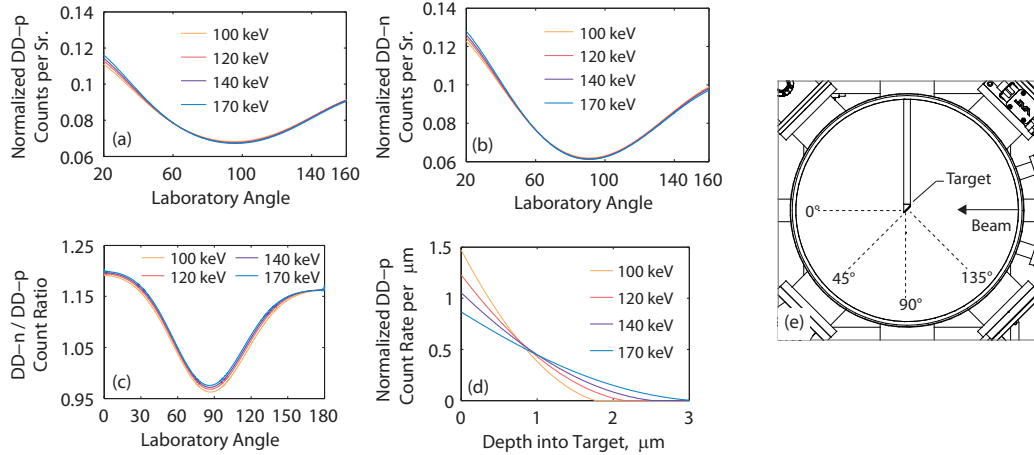


FIG. 9. Simulated results for a beam of deuterons (with four different energies) incident on an  $\text{ErD}_2$  target. The target forms an angle of  $45^\circ$  with respect to the beam, consistent with the lab setup shown in Fig. 8. Shown are (a) normalized DD-p counts per steradian as a function of laboratory angle (b) normalized DD-n counts per steradian as a function of laboratory angle (c) the DD-n/DD-p count ratio as a function of laboratory angle (d) normalized DD fusion reaction rate per  $\mu\text{m}$  as a function of depth into target and (e) Orientation of the beam and target inside the target chamber for these simulations.

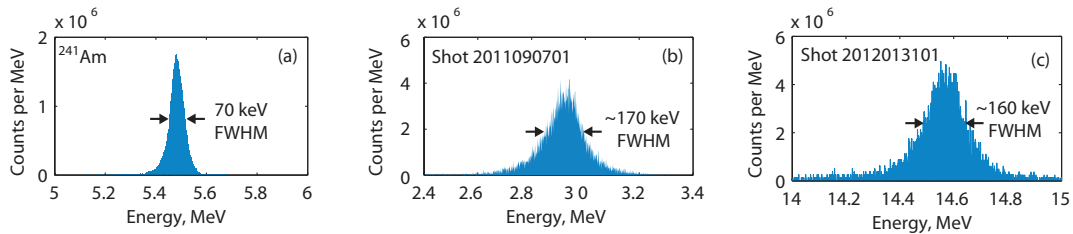


FIG. 10. Measured energy spectra for (a) an Americium-241 source (b) the LEIA DD proton source and (c) the LEIA  $\text{D}^3\text{He}$  proton source. The LEIA proton data were acquired with a  $6 \mu\text{m}$  Al filter placed in front of the SBD. The amount of line broadening due to this filter is small ( $\sim 20 \text{ keV}$ ) but the downshift is significant and must be taken into account for characterization of the mean proton energies. The americium source is used to infer the broadening due to the SBD, preamplifier and MCA. This instrument linewidth is then deconvolved from the measured linewidth of the fusion protons, shown here, in order to determine the linewidth of the fusion products source itself.



measured beam current is dominated by the ions of interest (typically  ${}^3\text{He}^+$  or D). Outputs of the simulation for practical cases are shown in Fig. 9. These simulations were made for 100 keV, 120 keV, 140 keV and 170 keV deuteron beams incident on an  $\text{ErD}_2$  target. The outputs are normalized to the total number of fusion counts per second to illustrate relative differences between beam energies.

As shown in Fig. 9a-c, the fluence of DD protons and neutrons peak towards the forward beam direction ( $0^\circ$  laboratory angle). The forward peaks in these plots are the result of the forward momentum introduced into the system by the deuteron beam. The ratio of DD-n to DD-p is essential for any associated-particle measurements. For these types of measurements, the DD neutron fluence at a given location in the target chamber is inferred by measurement of DD protons using an adjacent SBD. Correction factors must be applied between different laboratory angles to infer neutron yields properly. Corrections must also be applied for neutron scattering in the target chamber, as discussed in the next section. This technique has been used for neutron diagnostic development, as discussed in Sec. IV. Fig. 9d shows the normalized DD reaction rate as a function of target depth; as expected, reactions occur within a few microns corresponding to the range of the deuterons in  $\text{ErD}_2$ .

The beam-target physics code has also been used to obtain the expected energies of the charged fusion products at a given location in the target chamber and to understand the sources of line broadening for the 3 MeV and 14.7 MeV fusion-protons. The former is used to verify the MCA calibration, discussed in the previous section, while the latter is important for characterization of the instrumental linewidth of diagnostics being developed. The linewidth as measured by the SBD is due in part to the instrument response of the charged-particle diagnostics suite (SBD + preamp + MCA combination) and also due to beam-target physics. These two components must be quantified to determine what the actual incident linewidth is. This has been achieved by exposing the SBD to  $\alpha$ -particles from a  ${}^{241}\text{Am}$  source, as shown in as shown in Fig. 10a. The amount of broadening introduced by the charged-particle suite is  $\sim 70$  keV (FWHM). Shown in Figs. 10b-c are the energy spectra of DD and  $\text{D}^3\text{He}$  protons, respectively, as measured by the SBD at a distance of 14.5 cm from the fusion product source and an angle of  $90^\circ$  with respect to the 140 keV deuteron beam.

The mean energies of DD and  $\text{D}^3\text{He}$  protons, after they exit the target at  $90^\circ$  with respect to the beam, have been measured to be  $3.06 \pm 0.04$  MeV and  $14.58 \pm 0.04$  MeV, respectively.

This was achieved by fitting the measured spectra shown in Figs. 10b-c and then up-shifting the mean energies from the fit through the 6  $\mu\text{m}$  Al filter (placed in front of the SBD for these measurements). The mean values predicted by the beam-target simulation are 3.04 MeV and 14.67 MeV, which are within the statistical and systematic uncertainties associated with the measurement and calibration of the charged-particle suite. The actual linewidth of the fusion product source is the measured linewidth (Figs. 10b-c) after the instrumental linewidth has been deconvolved (Fig. 10a). After correcting for the instrumental width of  $\sim 70$  keV (FWHM), the linewidths of the DD and  $\text{D}^3\text{He}$  fusion-products source are  $\sim 150$  keV and  $\sim 140$  keV (FWHM). The beam-target simulation is able to account for approximately half of the source linewidth. Though it simulates kinematics and ranging of beam ions and fusion products in the target, the simulation does not include energy straggling or finite source size effects. We attribute the remainder of the unaccounted linewidth to these effects.

#### D. MCNP Simulations

The development of neutron diagnostics, in particular yield diagnostics, requires a thorough characterization of scattering effects in the target chamber. The Monte-Carlo simulation code MCNP<sup>22</sup> was used for this purpose. An accurate model of the target chamber itself, including all significant sources of scattering within the chamber, was used for this simulation; materials and geometry were specified from solid models. Simulations were conducted assuming an isotropic point source of DD neutrons with a birth energy of 2.45 MeV in the target. Figures 11a-b show a top and side view of the target chamber, with contours of normalized neutron fluence scaled by  $4\pi R^2$ ; deviations from unity thus represent a divergence from a  $1/r^2$  scaling. The black lines shown in the figure indicate the position of the water-cooled target holder and the target chamber walls. For the top view, shown in Fig. 11a, the D beam enters from the bottom, striking the target at a 45 angle. Similarly, in the side view, shown in Fig. 11b, the D beam enters normal to the figure into the page.

It is clear from these simulations that scattering corrections are significant, even for a large cylindrical target chamber (60 cm  $\times$  15 cm). The target, which is angled at 45°, casts a shadow along the entire chamber where the neutron fluence is significantly lower; the fluence generally increases as one approaches the target chamber wall, where it is enhanced by nearly 50%. On the non-shadow side, where neutron diagnostics are typically placed for calibration,

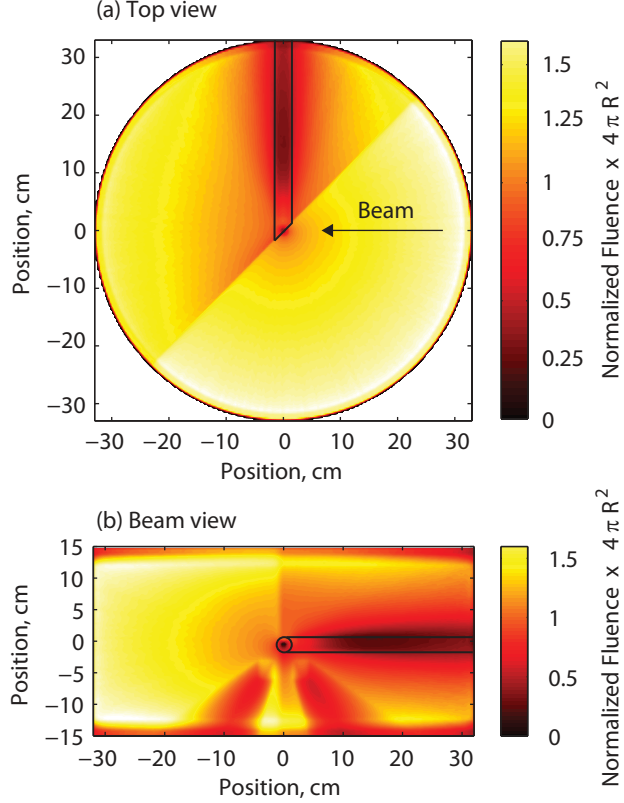


FIG. 11. MCNP simulation of neutron scattering within the LEIA target chamber showing (a) top view and (b) side view of the chamber. Shown are contours of normalized neutron fluence scaled by  $4 \pi r^2$ ; deviations from unity represent a divergence from a  $1/r^2$  scaling. The black lines indicate the water-cooled target. Significant correction factors must be applied to neutron yields inferred from diagnostics. At a distance of 10 cm from the target a correction factor of approximately 0.80 needs to be applied to the measured fluence to correctly infer the neutron yield from a local measurement.

significant corrections still need to be applied to experiments. Even at a distance of 10 cm from the source, the neutron fluence is enhanced by 20%. Neutron diagnostics are calibrated a few centimeters from the source. This choice minimizes the scattering correction, but is sufficiently far from the source that uncertainties in the absolute source position, typically 2 mm, are insignificant.

These detailed simulations of neutron scattering have been essential for the development and calibration of a CR-39-based neutron yield diagnostic used at both Omega and the NIF, as well as an indium activation-based yield diagnostic<sup>21,23</sup> developed by Sandia National Laboratories for use at Omega, Z and the NIF.

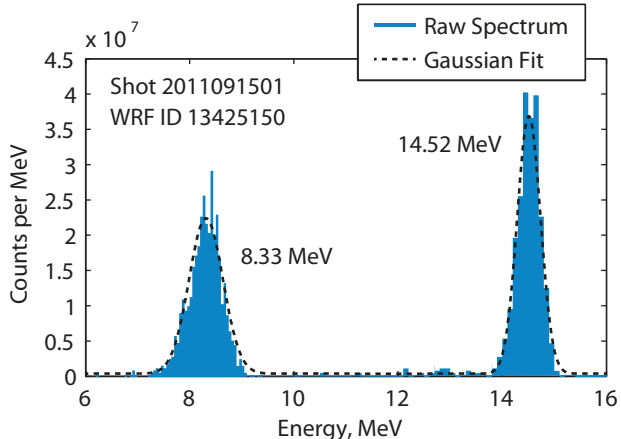


FIG. 12. WRF proton energy spectra acquired on LEIA. Each WRF is exposed to two populations of protons, each with well-known mean energies. The WRF is then calibrated using this data.

#### IV. DIAGNOSTICS DEVELOPMENT

A number of nuclear diagnostics have been developed, tested and calibrated using LEIA. In the past, LEIA has been primarily utilized for characterization of CR-39 solid-state nuclear track detectors, which form the basis for many nuclear diagnostics; these works have led to a number of publications on the CR-39 response to charged-particles<sup>24–26</sup> and coincidence counting with CR-39.<sup>27</sup> Over the last several years, an increasing amount of time has been spent calibrating diagnostics to better precision and developing other types of diagnostics; each of the diagnostics are briefly outlined in what follows.

##### A. Wedge-Range-Filter Spectrometers

Wedge-Range-Filter (WRF)<sup>28</sup> proton spectrometers are composed of an aluminum wedge positioned onto a piece of CR-39. The WRF spectrometers, capable of measuring proton spectra in the energy range of 4 MeV - 20 MeV, have been in use at Omega<sup>29,30</sup> for a number of years and have more recently been used on the NIF.<sup>31</sup> These spectrometers are routinely used to measure primary and secondary fusion yields, shell  $\rho R$  from the downshift of charged fusion products and fuel  $\rho R$  from scattered fuel ions (“knock-ons”).

After manufacture, the WRFs are calibrated and performance tested using the accelerator before they are sent out for use at Omega and the NIF. WRF proton energy spectra acquired on LEIA is shown in Fig. 12. WRFs are also periodically tested for surface de-

gradation between shots on the NIF. The aforementioned upgrades to the charged-particle diagnostics suite have recently allowed for more precise calibrations of the WRFs. Uncertainties in the energy calibration of WRFs are in the range of  $\pm 150$  keV and this has enabled new physics studies. For example, using multiple WRFs, it is now possible to study the P2/P0  $\rho R$  asymmetry mode in ICF implosions, in-flight, to a precision in P2/P0 of  $\pm 0.07$ . Techniques are also being developed to measure the fuel ion temperature ( $T_i$ ) using the line-width of charged-fusion products. The line width, as measured by the WRF, consists of several components, one of which is the doppler broadening due to finite  $T_i$ . To extract this component from the WRF data, the instrumental broadening due to the WRF itself must be well characterized. These studies are being carried out on LEIA.

## B. CR-39-based DD-n Yield Diagnostic

A novel, CR-39-based DD-neutron yield diagnostic, developed on LEIA and tested on OMEGA, measures absolute DD yields as well as the fraction of neutron backscatter at a given location<sup>32</sup>. The diagnostic (Fig. 13a) consists of a piece of CR-39 partially covered by a foil of 100  $\mu\text{m}$  thick polyethylene ( $\text{C}_2\text{H}_4$ ), which serves to enhance the neutron-induced proton signal on the CR-39 directly behind the foil. The uncovered CR-39 serves as a background region for subtraction of both intrinsic background and recoil protons produced in the CR-39 itself. The background-subtracted signal from the polyethylene-covered region of the CR-39 therefore measures only recoil protons generated in the polyethylene, and is directly proportional to the absolute neutron fluence. Furthermore, because only polyethylene-generated protons are detected, the detector is sensitive only to DD neutrons incident from the front, a distinct advantage over other neutron detectors that are susceptible to backscatter. By placing polyethylene behind as well as in front of the CR-39, it is possible to measure the relative amount of neutron backscatter (by comparing the polyethylene-produced signal on the back side to the polyethylene-produced signal on the front side).

The neutron detection efficiency and background subtraction methods used for this diagnostic were developed on LEIA using the associated particle technique, whereby the absolute DD-neutron fluence at the detector is inferred from the measured DD-proton fluence at an adjacent SBD. Sample data taken on LEIA is shown in Fig. 13b. In the top right cor-

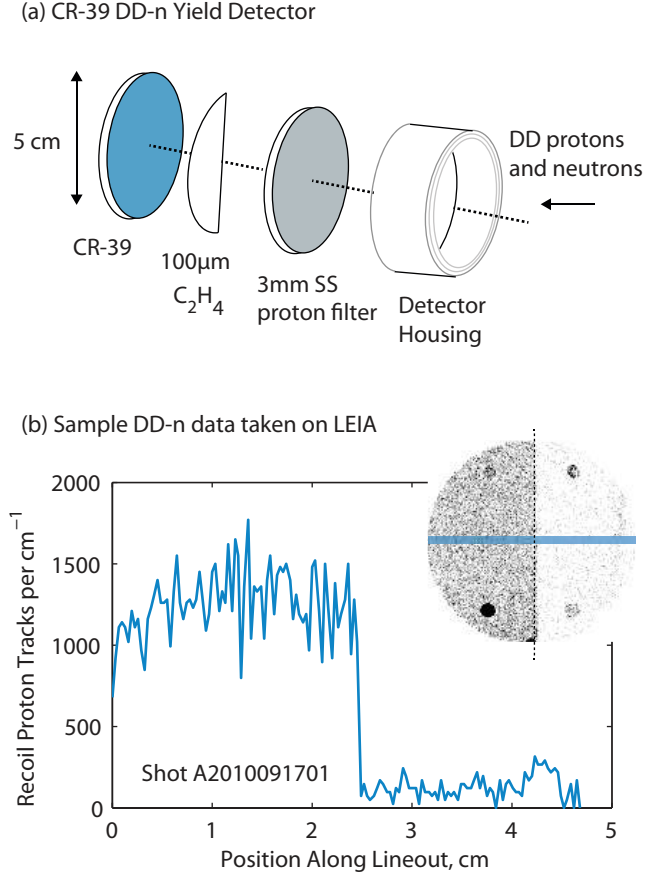


FIG. 13. (a) CR-39-based DD-n yield diagnostic components, including a 5 cm diameter aluminum housing, 3 mm thick stainless steel proton filter, 100  $\mu\text{m}$  polyethylene ( $\text{C}_2\text{H}_4$ ) neutron multiplier and the CR-39 detector (b) Image of CR-39 from a DD-n detector (top right corner), exposed to a known fluence of 2.45 MeV DD-n's on LEIA. In this image, darker pixels indicate regions of higher recoil protons; the four dark spots in the image are alignment fiducials. The detector was fielded with the left side of the CR-39 covered with 100  $\mu\text{m}$  of polyethylene ( $\text{C}_2\text{H}_4$ ). A horizontal lineout across the center of the detector is shown in the plot. Note the enhancement of recoil protons due to the polyethylene.

ner of the figure is an image of the CR-39 detector, with the left side covered with 100  $\mu\text{m}$  polyethylene. In this image, darker pixels represent a greater number of recoil proton tracks. Alongside the image is a lineout of proton fluence across the detector, which shows the enhancement of recoil protons due to the polyethylene. The neutron yield corresponding to this data is inferred from the adjacent SBD measurement, which must be corrected for neutron scattering, finite source size and kinematic differences in the DD-p and DD-n yields.

Thus, precise characterization of the fusion products source, as determined by the beam-target physics simulations, MCNP characterization of neutron scatter in the target chamber and the TVS diagnostic are central to development of this diagnostic. Several aspects of the diagnostic are still being developed,<sup>33</sup> including directionality of incident neutrons, effects of prolonged exposure to vacuum, and variability of CR-39 response to protons.

### C. Indium Activation Neutron Yield Diagnostic

The indium activation neutron yield diagnostic<sup>21,23</sup> relies on the activation and subsequent decay of the activated material to infer neutron yield at Z and the NIF. Indium “slugs” are activated during experiments by an unknown number of DD or DT neutrons through the reaction  $^{115}\text{In}(n,n')^{115m}\text{In}$ . The meta-stable  $^{115}\text{In}$  will then decay by emitting 336 keV gammas (the threshold energy for activation), which are measured using a high-purity germanium (HPGe) detector. A calibration factor, known as the  $F$  factor, relates the measured gamma yield to the total neutron yield.

The  $F$  factor is generally obtained through experimental calibration and encompasses detector efficiencies. Note that on Z, one must also consider the competing reaction,<sup>34</sup> which stems from the strong x-ray background:  $^{115}\text{In}(\gamma,\gamma')^{115m}\text{In}$ . Calibration of this diagnostic on LEIA is thus unique since  $F$  factors may be obtained for an x-ray free environment.

Preliminary experiments on LEIA were used to determine the  $F$  factors for a number of indium samples. Samples of various sizes were activated within approximately 30 minutes at DD reaction rates of about  $10^6$ . The samples were then removed from the target chamber within minutes of after the shot; the gammas were then counted using the HPGe. As in the case of the CR-39-based DD-n Yield Diagnostic, and as discussed in Secs. IIB and IIID, the target viewing system and simulation of neutron scattering were essential for precise determination of the  $F$  factor. In addition, stability of the fusion reaction rate is particularly important over these timescales. This is because the indium is continuously bombarded with neutrons for extended periods of time on LEIA. If the neutron flux is not stable, it is difficult to assign an  $F$  factor to the diagnostic. As discussed in Sec. IIA, recent improvements to the gas control system have stabilized the reaction rate significantly and will benefit future  $F$  factor experiments.

## D. Particle Time-of-Flight (pTOF) Diagnostic

The particle time-of-flight diagnostic (pTOF) is used at OMEGA and the NIF to measure the D-<sup>3</sup>He shock-bang and DD compression-bang time by resolving fusion protons and neutrons to an accuracy of  $\pm 150$  ps. The diagnostic consists of a chemical-vapor-deposited (CVD) diamond, biased to several hundred volts, and a filter in the front of the diamond to reduce the large x-ray background present in indirect-drive implosions at both OMEGA and the NIF. These measurements, when combined with the shock  $\rho R$  as measured by WRFs, strongly constrain implosion models. Improvements to the overall accuracy of the diagnostic are therefore essential to the ignition effort.

One improvement that will be implemented at the NIF is to increase the bias voltage on the detector. In addition to improving the response-time of the diagnostic, saturation effects that may be caused by the large hohlraum x-ray signal will be reduced. Various bias voltages are being tested on the accelerator before such a capability is implemented at the NIF.

Critical to the interpretation of the pTOF data is a thorough understanding of the instrument response function and sensitivity to protons. Single-particle and integrated charge studies are being conducted on the accelerator by ranging down 14.7 MeV protons to energies of interest. The charged-particle diagnostics suite is essential in calibrating pTOF to the SBD during integrated charge studies. Moreover, the accelerator does not generate hard x-rays, allowing these studies to be carried out without an x-ray background.

## V. CONCLUSION

The MIT Linear Ion Accelerator (LEIA) has undergone several upgrades, which have improved our capability to develop advanced diagnostics for Omega, Z and the NIF. Implementation of a new ion source and custom gas control system now provides better regulation and improved stability of the fusion-product source. The addition of a new charged-particle data acquisition system has allowed for more precise energy characterization of the fusion products and therefore better calibration of charged-particle diagnostics. In-situ measurements of the on-target beam profile, made with a CCD camera, together with simulations of neutron scattering within the target chamber, have facilitated the development of neutron



yield diagnostics. These improvements, implemented largely by graduate and undergraduate students, allow better support of existing diagnostics and the development of new diagnostics in aid of the national program.

## ACKNOWLEDGMENTS

The authors thank the technical staff at the PSFC, in particular Bill Forbes, Ed Fitzgerald and Robert A. Childs, for engineering assistance. This work was done in part for the graduate student authors' PhD theses and was supported in part by Sandia National Laboratory (Agreement No. 611557), National Laser User's Facility (DOE Award No. DE-NA0000877), Fusion Science Center (Rochester Sub Award PO No. 415023-G), US DOE (Grant No. DE-FG52-09NA29553), Laboratory for Laser Energetics (LLE) (No. 414090-G), Lawrence Livermore National Laboratory (No. B580243)

## REFERENCES

- <sup>1</sup>J. Lindl. ICF: Recent Achievements and Perspectives. *Il Nuovo Cimento A (1971-1996)*, 106(11):1467–1487, 1993.
- <sup>2</sup>T. C. Sangster, R. L. McCrory, V. N. Goncharov, D. R. Harding, S. J. Loucks, P. W. McKenty, D. D. Meyerhofer, S. Skupsky, B. Yaakobi, B. J. MacGowan, L. J. Atherton, B. A. Hammel, J. D. Lindl, E. I. Moses, J. L. Porter, M. E. Cuneo, M. K. Matzen, C. W. Barnes, J. C. Fernandez, D. C. Wilson, J. D. Kilkenny, T. P. Bernat, A. Nikroo, B. G. Logan, S. Yu, R. D. Petrasso, J. D. Sethian, and S. Obenschain. Overview of inertial fusion research in the united states. *Nuclear Fusion*, 47:S686 – S695, 2007.
- <sup>3</sup>T. R. Boehly, D. L. Brown, R. S. Craxton, R. L. Keck, J. P. Knauer, J. H. Kelly, T. J. Kessler, S. A. Kumpan, S. J. Loucks, S. A. Letzring, F. J. Marshall, R. L. McCrory, S. F. B. Morse, W. Seka, J. M. Soures, and C. P. Verdon. Initial Performance Results of the OMEGA Laser System. *Optics Communications*, 133(1-6):495–506, 1997.
- <sup>4</sup>R. L. McCrory, R. E. Bahr, R. Betti, T. R. Boehly, T. J. B. Collins, R. S. Craxton, J. A. Delettrez, W. R. Donaldson, R. Epstein, J. Fenje, V. Yu. Glebov, V. N. Goncharov, O. V. Gotchev, R. Q. Gram, D. R. Harding, D. G. Hicks, P. A. Jaanimagi, R. L. Keck, J. H. Kelly, J. P. Knauer, C. K. Li, S. J. Loucks, L. D. Lund, F. J. Marshall, P. W. McKenty,

- D. D. Meyerhofer, S. F. B. Morse, R. D. Petrasso, P. B. Radha, S. P. Regan, S. Roberts, F. Séguin, W. Seka, S. Skupsky, V. A. Smalyuk, C. Sorce, J. M. Soures, C. Stoeckl, R. P. J. Town, M. D. Wittman, B. Yaakobi, and J. D. Zuegel. OMEGA ICF Experiments and Preparation for Direct Drive Ignition on NIF. *Nuclear Fusion*, 41(10):1413 – 1422, 2001.
- <sup>5</sup>S. C. McDuffee, J. A. Frenje, F. H. Séguin, R. Leiter, M. J. Canavan, D. T. Casey, J. R. Rygg, C. K. Li, and R. D. Petrasso. An accelerator based fusion-product source for development of inertial confinement fusion nuclear diagnostics. *Review of Scientific Instruments*, 79(4):043302, 2008.
- <sup>6</sup>M. C. Borras, K. W. Wenzel, D. H. Lo, R. D. Petrasso, D. A. Pappas, C. K. Li, and J. W. Coleman. 14 MeV Neutron Yields from D-T Operation of the MIT Cockcroft-Walton Accelerator. *Journal of Fusion Energy*, 12:317–322, 1993. 10.1007/BF01079676.
- <sup>7</sup>K. W. Wenzel, D. H. Lo, R. D. Petrasso, J. W. Coleman, C. K. Li, J. R. Lierzer, C. Borras, T. Wei, E. Hsieh, and T. Bernat. A fusions product source. 63(10):4837–4839, 1992.
- <sup>8</sup>National Electrostatics Corp. see <http://www.pelletron.com/>.
- <sup>9</sup>Glassman High Voltage Incorporated. see <http://www.glassmanhv.com/>.
- <sup>10</sup>Acromag, Inc. see <http://www.acromag.com/>.
- <sup>11</sup>Horiba STEC. see <http://www.horiba.com/semiconductor>.
- <sup>12</sup>MKS Instruments. see <http://www.mksinst.com/>.
- <sup>13</sup>D.J. Malbrough, D.K. Brice, D.F. Cowgill, J.A. Borders, L.A. Shope, and J.M. Harris. Deuteron stopping cross sections in transition metal hydrides. *Nuclear Instruments and Methods in Physics Research Section B: Beam Interactions with Materials and Atoms*, 28(4):459 – 469, 1987.
- <sup>14</sup>Axis Communications. see <http://www.axis.com/>.
- <sup>15</sup>N Sinenian, A. B. Zylstra, M. Manuel, J. A. Frenje, and R. D. Petrasso. A multithreaded modular software toolkit for control of complex experiments. *Computing in Science and Engineering*, 2011. To be submitted.
- <sup>16</sup>GIMP Toolkit. see <http://www.gtk.org/>.
- <sup>17</sup>Oracle MySQL Community Edition. see <http://www.oracle.com>.
- <sup>18</sup>C.A.E.N. see <http://www.caen.it/>.
- <sup>19</sup>Valentin T. and Jordanov. Deconvolution of pulses from a detector-amplifier configuration. *Nuclear Instruments and Methods in Physics Research Section A: Accelerators*,

- Spectrometers, Detectors and Associated Equipment*, 351(2-3):592 – 594, 1994.
- <sup>20</sup>Kenneth S. Krane. *Introductory Nuclear Physics, 3rd Edition*. Wiley, 1987.
- <sup>21</sup>C. L. Ruiz, R. J. Leeper, F. A. Schmidlapp, G. Cooper, and D. J. Malbrough. Absolute calibration of a total yield indium activation detector for dd and dt neutrons. 63(10):4889–4891, 1992.
- <sup>22</sup>Monte Carlo N-Particle (MCNP) Transport Code. see <http://mcnp-green.lanl.gov/>.
- <sup>23</sup>G. W. Cooper and C. L. Ruiz. NIF total neutron yield diagnostic. 72(1):814–817, 2001.
- <sup>24</sup>N. Sinenian, M. J. Rosenberg, M. Manuel, S. C. McDuffee, D. T. Casey, A. B. Zylstra, H. G. Rinderknecht, M. Gatu Johnson, F. H. Séguin, J. A. Frenje, C. K. Li, and R. D. Petrasso. The response of CR-39 nuclear track detector to 1-9 MeV protons. 82(10):103303, 2011.
- <sup>25</sup>A. B. Zylstra, H. G. Rinderknecht, N. Sinenian, M. J. Rosenberg, M. Manuel, F. H. Séguin, D. T. Casey, J. A. Frenje, C. K. Li, and R. D. Petrasso. Increasing the energy dynamic range of solid-state nuclear track detectors using multiple surfaces. 82(8):083301, 2011.
- <sup>26</sup>M. J.-E. Manuel, M. J. Rosenberg, N. Sinenian, H. Rinderknecht, A. B. Zylstra, F. H. Séguin, J. Frenje, C. K. Li, and R. D. Petrasso. Changes in cr-39 proton sensitivity due to prolonged exposure to high vacuums relevant to the national ignition facility and omega. 82(9):095110, 2011.
- <sup>27</sup>D. T. Casey, J. A. Frenje, F. H. Séguin, C. K. Li, M. J. Rosenberg, H. Rinderknecht, M. J.-E. Manuel, M. Gatu Johnson, J. C. Schaeffer, R. Frankel, N. Sinenian, R. A. Childs, R. D. Petrasso, V. Yu. Glebov, T. C. Sangster, M. Burke, and S. Roberts. The coincidence counting technique for orders of magnitude background reduction in data obtained with the magnetic recoil spectrometer at OMEGA and the NIF. 82(7):073502, 2011.
- <sup>28</sup>F. H. Séguin, J. A. Frenje, C. K. Li, D. G. Hicks, S. Kurebayashi, J. R. Rygg, B. E. Schwartz, R. D. Petrasso, S. Roberts, J. M. Soures, D. D. Meyerhofer, T. C. Sangster, J. P. Knauer, C. Sorce, V. Yu Glebov, C. Stoeckl, T. W. Phillips, R. J. Leeper, K. Fletcher, and S. Padalino. Spectrometry of charged particles from inertial-confinement-fusion plasmas. *Review of Scientific Instruments*, 74(2):975–995, 2003.
- <sup>29</sup>F. H. Séguin, C. K. Li, J. A. Frenje, D. G. Hicks, K. M. Green, S. Kurebayashi, R. D. Petrasso, J. M. Soures, D. D. Meyerhofer, V. Yu Glebov, P. B. Radha, C. Stoeckl, S. Roberts, C. Sorce, T. C. Sangster, M. D. Cable, K. Fletcher, and S. Padalino. Using secondary-proton spectra to study the compression and symmetry of deuterium-filled capsules at

- omega. *Physics of Plasmas*, 9(6):2725–2737, 2002.
- <sup>30</sup>J. A. Frenje, C. K. Li, F. H. Séguin, S. Kurebayashi, R. D. Petrasso, J. M. Soures, J. Delettrez, V. Yu. Glebov, D. D. Meyerhofer, P. B. Radha, S. Roberts, T. C. Sangster, S. Skupsky, and C. Stoeckl. Measurements of fuel and shell areal densities of omega capsule implosions using elastically scattered protons. *Physics of Plasmas*, 9(11):4719–4725, 2002.
- <sup>31</sup>J. A. Frenje, C. K. Li, J. R. Rygg, F. H. Séguin, D. T. Casey, R. D. Petrasso, J. Delettrez, V. Yu. Glebov, T. C. Sangster, O. Landen, and S. Hatchett. Diagnosing ablator rho r and rho r asymmetries in capsule implosions using charged-particle spectrometry at the national ignition facility. *Physics of Plasmas*, 16(2):022702, 2009.
- <sup>32</sup>J. A. Frenje, C. K. Li, F. H. Séguin, D. G. Hicks, S. Kurebayashi, R. D. Petrasso, S. Roberts, V. Yu Glebov, D. D. Meyerhofer, T. C. Sangster, J. M. Soures, C. Stoeckl, C. Chiritescu, G. J. Schmid, and R. A. Lerche. Absolute measurements of neutron yields from dd and dt implosions at the omega laser facility using cr-39 track detectors. *Review of Scientific Instruments*, 73(7):2597–2605, 2002.
- <sup>33</sup>et al. F. H. Séguin. To be submitted. *Rev. Sci. Instrum.*
- <sup>34</sup>R. J. Leeper, C. L. Ruiz, G. A. Chandler, G. W. Cooper, D. E. Bower, D. N. Fittinghoff, E. C. Hagen, J. R. Hollaway, I. J. McKenna, L. A. McPherson, M. J. May, B. T. Meeham, A. J. Nelson, T. S. Perry, J. L. Porter, L. L. Robbins, D. B. Sinars, J. A. Torres, and L. H. Ziegler. Zr neutron diagnostic suite. *Journal of Physics: Conference Series*, 112(3):032076, 2008.